Analytic control law for a food storage room

S. van Mourik, H. Zwart, University of Twente,
K.J. Keesman*, Wageningen University, The Netherlands

Corresponding author: S. van Mourik
Department of Applied Mathematics
University of Twente, The Netherlands
Phone: +31 (53) 489 3473 , Fax: +31 (53) 489 3800
e-mail: s.vanmourik@ewi.utwente.nl
* Systems & Control Group
Wageningen University, The Netherlands
e-mail: Karel.Keesman@wur.nl

Abstract A bulk of agricultural products, such as potatoes, onions, or fruits is normally stored in a climate controlled room. The products produce heat due to respiration. A ventilator blows cooled air around to keep the products at a steady temperature to prevent spoilage. We model this room by a set of nonlinear coupled partial differential equations (p.d.e.'s). Due to the complexity of this model, we need to simplify it to design an open loop control law. We propose an input that switches between discrete values, which results in a (piecewise) linear model. The system states can be decomposed in very slow and very fast states, and the fast state dynamics can be neglected. A third model simplification is made by approximation of a transcendental transfer function by a low-order rational one. The control problem, that consists of the determination of the switching moment, can now be solved analytically. We also derive an analytic expression for the time needed to cool down the bulk from an arbitrary initial temperature. The analytical form of the solutions provides a lot of physical insight and allows us to derive some design rules.

1 Introduction

A large volume of perishable foods that are stored consists of bulk stored foods, such as potatoes and onions. The storage time ranges from a month to almost a year. Harvested products are living organisms that produce heat, transpire, and produce ethylene and CO_2. Therefore, the control parameters for maintaining the food quality are temperature, humidity, ethylene concentration, and CO_2 concentration. Too much ethylene and CO_2 accelerates the spoilage [16]. This is prevented by ventilation with outside air, most often once a day. In general, the temperature control is done in two ways; ventilation with outside air, or by means of a heat exchanger. Furthermore, a fan enforces the air circulation. For most harvested products, the optimal relative humidity is relatively high, to prevent weight losses, and since the products themselves transpire, this condition is usually satisfied in closed storage rooms. Therefore, daily ventilation with air slightly cooler than the product temperature not only reduces the ethylene and CO_2 concentrations, but also avoids too high relative humidities and condensation. However, the optimal air temperature inside is less easy to

realize, since the outside temperature is often much higher than the product temperature (especially in autumn and spring). Moreover, as mentioned before, the products respirate, i.e., produce heat.
The temperature of the products in the bulk varies spatially. Usually, cold air flows upwards through the bulk. Inside the bulk, the air warms up and consequently the products at the top will be some degrees warmer than those at the bottom. Therefore it is not a trivial task to develop a control algorithm that keeps the products in the bulk at a constant, desired temperature. For detailed information, see [15].
There is extensive literature available about the modelling aspects of bulk storage rooms. In [11, 21] the main goal is to derive a model describing the dynamics of the enthalpy that is suitable for control design. Extensive CFD models are proposed in [13, 2, 3, 24, 23], and experimental validation studies were done in [13, 2, 24, 23]. In [20] a review of different CFD modelling approaches is given. There is a considerable amount of literature concerning control of nonlinear distributed parameter systems with applications to chemical and process engineering, for example [1, 6, 5] and the review article of [4]. However, there is not a vast amount of literature on control design for bulk storage rooms. In [7] a fuzzy controller was tested on a mathematical model. Gottschalk proposed in [8] a sensor based control law for a bulk storage room ventilated with outside air, and constructed in [9] a fuzzy controller. The controller was tested experimentally. For sensor based control design, the control algorithms are relatively easy implementable in practice. However, since these types of control laws are not model based, less physical interpretation and insight of the controlled process is obtained than for model based controllers. Keesman et al [10] used a model predictive control (MPC) algorithm for the temperature and humidity control of a bulk storage room with outside air ventilation. Verdijck [21] proposed an MPC algorithm for the control of temperature, moist-, and sugar content of potatoes in a bulk storage room with outside air ventilation. Both proposed algorithms are model based and were tested by simulation studies using real weather conditions. The aim of the algorithms was to keep temperature and humidity within bounds at low economic costs. Due to the rather high complexity of the models, model based control design requires computer simulation studies. While the outcomes and predictions are often accurate enough, this method has some considerable drawbacks. Complex numerical simulations are always very time consuming, both due to software programming and demand on computer capacity. The information that simulations give, can be detailed and accurate, but always hold for a particular parameter choice. Consequently, a large part of the physical interpretation and insight is lost. Also, in practice, these control algorithms require complex control technology and software. It is therefore desirable to reduce these models, or model components, in complexity.
The main goal of this paper is to derive a simplified model that preserves the prior physical knowledge and which is suitable for standard linear control design. This opens the door for deriving guidelines regarding storage room design in a computationally easy way, as is shown in [18]. The approximation technique that is proposed here could also help with the simplification of the complex

models used for MPC. Further, in [19] a PI controller that is based on the approximated model in this paper, is designed. It should also be noted that this research on bulk stored food could be a starting point for more advanced storage of vulnerable agricultural products, such as packed foods.
The structure of this paper consists of the following three steps, see Figure 1. First, we derive a basic model for the heat transport inside the storage room. We make some assumptions to keep the model as simple as possible without losing the essential physical properties. The resulting model in terms of a nonlinear p.d.e. is validated by experimental results
Second, the inputs are assumed to be constant. The control problem consists now of the determination of the moment to switch between the inputs. Between two input switches, the system is linear, and the system dynamics are mathematically approximated by means of a transfer function approximation and timescale decomposition. This ultimately leads to a low order linear model.
Third, a control law is derived analytically. Also, the time that the products need to cool down after the harvest (the settle time for the bulk temperature) is derived analytically. The organization of the paper is as follows. In Subsection

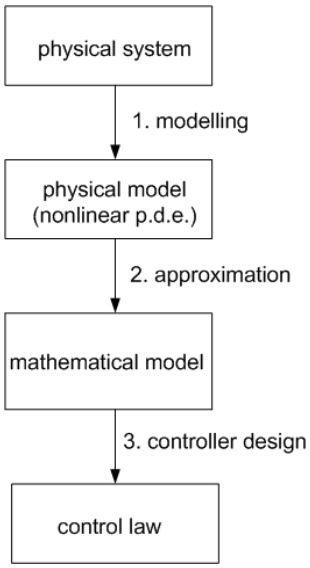

Figure 1: The proposed solution procedure.

2.1 some physical assumptions are made, and a model is derived. In Subsection 2.2 a model simplification is done by fixing the input and approximating a p.d.e. with a first order ordinary differential equation (o.d.e.). The resulting model is referred to as the nominal model. In section 3 the nominal system is validated experimentally. The nominal model is shown to be reasonably accurate. In Section 5, the fast dynamics of the air temperatures is neglected. Using this simplification, the settle time for the bulk temperature after the harvest is

calculated. The timescale separation, and the transfer function approximation result in a first order, linear model. In Section 6 an open-loop control law, that consists of the optimal switching time between the discrete inputs, is based on this model, and tested on the nominal model. Simulations show that the control law works very accurately, which validates the model simplifications. In Section 7 we briefly discuss the results.

2 The model

2.1 Physical model

We consider a closed storage room with a bulk of products, as depicted in Figure 2. Given the large amount of data available in literature, we consider potato as specific product. The air temperatures $T_a(x,t)$ and $T_0(t)$ are regulated by a fan

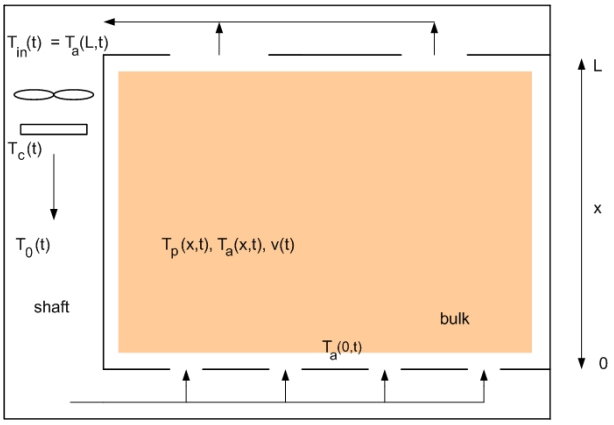

Figure 2: Schematic representation of a bulk storage room

that blows the air through the shaft and through the bulk. A cooling element, with variable temperature $T_c(t)$, is placed right below the fan. The air flux induced by the fan, and the temperature of the cooling element are the control inputs. The controlled variable is the product temperature $T_p(x,t)$. The aim is now to design a control law such that $T_p(x,t)$ at $x = L$ is kept at a constant, desired level. The following assumptions were made:

1. The air- and product temperature in the bulk, T_a and T_p, only vary with the height of the bulk, so they are uniform w.r.t. the width.
2. The walls are perfectly insulated.
3. The air temperature in the shaft and under the floor, $T_0(t)$, is well-mixed and therefore spatially uniform.
4. The temperature dynamics of the air between the top of the bulk and the fan is neglected.

5. No effects of moisture transport are incorporated. However, the heat capacity of air is adjusted for a high humidity.

6. The products are spherical.

7. The product skin has the same heat conduction as the product interior.

8. The whole product surface is exposed to air.

9. There is no bulk conduction, i.e., there is no heat exchange between the products.

10. Diffusion in the air is neglected.

The motivation and the restrictiveness of each assumption are discussed below.

1. This is a restrictive assumption, since incorporating temperature gradients in more than one direction, would require a far more complex model, due to a nonuniform airflow.

2. In [18] the model is extended with heat transport through the walls, which makes the analysis in the following sections somewhat more laborious.

3. A spatial model for $T_0(t)$ would not alter the analysis, but the expressions would get more involved.

4. This can be accounted for by adding an extra equation for the state variable T_{in}.

5. Including moisture transport complicates the model drastically, and seems to make a linearization necessary to make the analysis below possible.

6. This assumption makes the derivation of transfer functions easier. However, since the product temperature dynamics are approximated by a lumped model, other shapes with a suitable hydraulic diameter are also allowed, see [17].

7. This simplifies the analysis in the next section, and since the product temperatures are lumped later on, this has no further influence.

8. The contact with other product surface can easily be accounted for, but it is unknown to the authors. Since it is small, it will have negligible influence on the heat transport. This is checked by simulations while varying the total product surface.

9. The ratio of heat exchange between air and products, and heat exchange between products by means of conduction, is

$$\frac{hA_1(T_p(R) - T_a)}{\lambda_a A_2 \frac{\partial T_p}{\partial x}} \approx \frac{hA_1 2R(T_p(R) - T_a)}{\lambda_a A_2 (T_{p,1} - T_{p,2})} \gg 1. \tag{1}$$

Here, A_1 is the product surface per bulk volume that contacts the air, A_2 the product surface per bulk volume not contacting the air, $T_p(R)$ the product surface temperature, R the product radius, and $T_{p,1}$ and $T_{p,2}$ temperatures of two products that lie next to each other. $T_{p,1} - T_{p,2}$ and $T_p(R) - T_a$, are supposed to be of the same order, as well as $A_1 2R$ and A_2. Because for forced convection h is 10 to 100 times larger than λ, heat transport inside the bulk will be convection-dominated. With bulk conduction it was not possible to derive an analytical expression for the open loop controller.

10. This is justified by the fact that the Péclet number (that indicates the ratio of convection over diffusion)

$$\mathrm{Pe} = \frac{v d \rho_a c_a}{\lambda_a} \gg 1. \tag{2}$$

Here v is the air velocity, d the diameter of the pores, ρ_a the air density, c_a the heat capacity of air, and λ_a the heat conduction of the air. A list of all symbols is given in the Appendix.

The assumptions lead to the following energy balance. The energy inflow of the air in the fan shaft is modelled in a basic way: $\rho_a c_a \Phi(\alpha T_c(t) + (1-\alpha)T_{in}(t))$, with c_a the heat capacity of air, and Φ the flux of air through the shaft. The dimensionless α denotes the effectiveness of the cooling device: $\alpha = 1$ implies that the incoming air $T_{in}(t)$ is totally cooled down (or heated up) to the temperature of the cooling element, $T_c(t)$, while $\alpha = 0$ implies that the incoming air is not cooled at all. In [18] the relation between α and Φ was experimentally determined. Without loss of generality we assume that α is constant. Because of the perfect insulation of the walls, we have that $T_{in}(t) = T_a(L,t)$. The energy outflow equals $-\rho_a c_a \Phi T_0(t)$. The dynamic energy balance for $T_0(t)$ therefore becomes

$$\begin{aligned} \rho_a c_a V \frac{\partial T_0(t)}{\partial t} =& -\rho_a c_a \Phi \alpha \Big(T_a(L,t) - T_c(t) \Big) \\ & + \rho_a c_a \Phi T_a(L,t) - \rho_a c_a \Phi T_0(t), \end{aligned} \tag{3}$$

with V the volume of the shaft.
The energy balance for $T_a(x,t)$ is, with $x \in (0,L)$,

$$\begin{aligned} \rho_a c_a \gamma \frac{\partial T_a(x,t)}{\partial t} =& -\gamma \rho_a c_a v \frac{\partial T_a(x,t)}{\partial x} \\ & + h(v) A_{ps} \Big(T_p(R,x,t) - T_a(x,t) \Big), \end{aligned} \tag{4}$$

with boundary condition

$$T_a(0,t) = T_0(t). \tag{5}$$

Here, A_{ps} is the product surface area that is exposed to air per bulk volume, and $T_p(R,x,t)$ is the product surface temperature at x. The two r.h.s. terms

in (4) denote the convection of heat and the heat exchange between product surface and air, respectively. The heat transfer coefficient h depends on v via the implicit relation (see [22])

$$\mathrm{Nu} = (0.5\mathrm{Re}^{1/2} + 0.2\mathrm{Re}^{2/3})\mathrm{Pr}^{1/3}, \quad 10 < \mathrm{Re} < 10^4 \tag{6}$$

with Nu, Re and Pr the Nusselt, Reynolds and Prandtl number respectively, which are functions of v and h, see Appendix A.2. The heat transport inside a product at height x is modelled by diffusion in a sphere with radius R.

$$\begin{aligned}\rho_p c_p \frac{\partial T_p(r,x,t)}{\partial t} =& \lambda_p \frac{1}{r^2}\frac{\partial}{\partial r}\left(r^2 \frac{\partial T_p(r,x,t)}{\partial r}\right) \\ &+ \rho_p \tilde{a} T_p(r,x,t) + \rho_p b,\end{aligned} \tag{7}$$

where ρ_p, c_p, and λ_p are the product density, heat capacity, and conductivity, respectively. The last two terms in equation (7) denote the heat production, see [24] and the references therein. The boundary conditions are

$$\frac{\partial T_p}{\partial r}(0,x,t) = 0 \text{ by symmetry at the origin} \tag{8}$$

$$\lambda_p \frac{\partial T_p}{\partial r}(R,x,t) = h(v)(T_a(x,t) - T_p(R,x,t)) \tag{9}$$

The second equation denotes the heat flux through the product surface. The values of a and b in equation (7) are used in [23], and fit the experimental data in [15] well for $T_p > 278\ K$. To simplify the analysis in the next sections, the heat production is approximated as $\tilde{a}T_p + b = aT_p$, with equality in $T_p = 280\ K$. We impose the following additional assumption

- $T_p(r,x,t)$ is regarded as a porous medium in x. The heat flux between air and products at x is modelled as the flux between a sphere with air temperature $T_a(x,t)$ along its surface.

The equations are nonlinear since v enters equation (3) by $\Phi = A_f v \gamma$ (with A_f the surface of the bulk floor, and γ the bulk porosity), equation (4) via the implicit relation (6), and equation (7) via equation (9). The full system

dynamics together with boundary conditions is described by

$$\begin{aligned}
\frac{\partial T_0(t)}{\partial t} &= -\frac{\Phi}{V}\alpha(T_a(L,t) - T_c(t)) \\
&\quad + \frac{\Phi}{V}T_a(L,t) - \frac{\Phi}{V}T_0(t) && (10)\\
\frac{\partial T_a(x,t)}{\partial t} &= -v\frac{\partial T_a(x,t)}{\partial x} \\
&\quad + M_4\Big(T_p(x,t) - T_a(x,t)\Big) && (11)\\
T_a(0,t) &= T_0(t) && (12)\\
\frac{\partial T_p(r,x,t)}{\partial t} &= M_1\frac{1}{r^2}\frac{\partial}{\partial r}\left(r^2\frac{\partial T_p(r,x,t)}{\partial r}\right) \\
&\quad + M_2 T_p(r,x,t) && (13)\\
\frac{\partial T_p}{\partial r}(0,x,t) &= 0 && (14)\\
\frac{\partial T_p}{\partial r}(R,x,t) &= \frac{h(v)}{\lambda_p}\Big(T_a(x,t) - T_p(R,x,t)\Big), && (15)
\end{aligned}$$

with $M_1 = \frac{\lambda_p}{\rho_p c_p}$, $M_2 = \frac{a}{c_p}$, $M_4 = \frac{h(v)A_p}{\gamma\rho_a c_a}$, and appropriate initial conditions. This model will be referred to as the basic model. The controlled variable is T_p, and the control inputs are v and T_c.

2.2 Model approximation

In what follows, we assume the inputs to be piecewise constant. For fixed v, the system described by equations (10)–(15) becomes linear. Hence, in the frequency or Laplace domain the heat transfer between the air and the product surface can be written as

$$\widehat{T}_p(R,x,s) = G_p^R(s)\widehat{T}_a(x,s). \tag{16}$$

The transfer function $G_p^R(s)$ is a transcendental function and is approximated by a rational one. As rational approximation we choose the Padé[0,1] approximation in $s = 0$, so

$$G_p^R(s) \approx \frac{a_1}{a_2 + a_3 s}. \tag{17}$$

Because of the rational form we can transform (16)–(17) back into the time domain

$$\begin{aligned}
\frac{\partial T_p(R,x,t)}{\partial t} &= -\frac{a_2}{a_3}T_p(R,x,t) + \frac{a_1}{a_3}T_a(x,t) && (18)\\
&= A_p T_p(R,x,t) + B_p T_a(x,t), && (19)
\end{aligned}$$

with

$$\begin{aligned} a_1 &= \mathrm{Bi} \\ a_2 &= 2M_3 \cot(M_3) - 2 + \mathrm{Bi} \\ a_3 &= \frac{R^2}{M_1}\cot^2(M_3) + \frac{R^2}{M_1} - \frac{M_3}{M_2}\cot(M_3). \\ M_1 &= \frac{\lambda_p}{\rho_p c_p};\ \text{diffusion coefficient}\ \ (m^2/s) \\ M_2 &= \frac{a}{c_p};\ \text{reaction constant}\ \ (1/s) \\ M_3 &= \sqrt{M_2/M_1}R. \end{aligned} \tag{20}$$

The dimensionless parameter M_3, which indicates the heat production rate over the diffusive heat transfer rate, is analogous to the Thiele modulus

$$\mathrm{Th} = \frac{\text{chemical reaction rate}}{\text{diffusive mass transfer rate}}, \tag{21}$$

and Bi is the Biot number, which depends on v. Using the Padé approximation, the approximated system becomes

$$\begin{aligned} \frac{\partial T_0(t)}{\partial t} &= -\frac{\Phi}{V}\alpha(T_a(L,t) - T_c(t)) \\ &\quad + \frac{\Phi}{V}T_a(L,t) - \frac{\Phi}{V}T_0(t) \qquad (22) \\ \frac{\partial T_a(x,t)}{\partial t} &= -v\frac{\partial T_a(x,t)}{\partial x} \\ &\quad + M_4\Big(T_p(x,t) - T_a(x,t)\Big) \qquad (23) \\ \frac{\partial T_p(R,x,t)}{\partial t} &= A_p T_p(R,x,t) + B_p T_a(x,t) \qquad (24) \\ T_a(0,t) &= T_0(t). \qquad (25) \end{aligned}$$

Starting from the full system, this model approximation comes down to a heat transfer model inside a porous medium, which is done for example in [10, 11]. The difference is that here there is no bulk conduction. From now on we refer to system (22)–(25) as the nominal model.

3 Model validation by experiment

In [12] and [24] experimental data was reported from an experiment in which a forced laminar airflow cools down a column filled with a bulk of potatoes of 15.5 ^oC. A constant laminar airflow of 6.7 ^oC was forced through the column for 92 hours. The physical properties of that experiment are listed in Table 1. The specific area of potato was not reported. From the average size (length

95 mm, diameter 51 mm), the potato density (1014 kg/m^3 according to [11]), and the total weight of the bulk (360 kg), it follows that the column was filled with approximately 3000 potatoes. The total product surface exposed to air, assuming this is 95 % of the total product surface, is 41 m^2 per m^3 bulk. In [24] a model that incorporates heat transfer by moisture transport is used, and this model predicts the experimental bulk temperatures very well. The experiment is simulated by our model using $T_c(t) = 6.7\ ^oC$, $\alpha = 1$, and $V = 0$, such that $T_0(t) = 6.7\ ^oC$. Table 2 shows the experimental air temperatures at the top, the middle, and the bottom of the bulk, and the predicted temperatures by system (22)–(25) at different times. According to [24], the complex temperature dynamics between the bottom and middle of the bulk are caused by evaporation effects. Our model predictions match the experimental data reasonably well. In the middle of the bulk the predictions are least accurate. Our model predicts higher temperatures compared to the experiment, and the model proposed in [24]. This is probably due to the heat loss by evaporation that was neglected in our model. Nevertheless, we conclude that our model is reasonably accurate.

c_a	1.7 10^3 $J/kg\ K$	A_f	0.3848 m^2
c_p	3.52 10^3 $J/kg\ K$	R	0.0325 m
Φ	2.6 10^{-3} m^3/s	L	2.4 m
v	0.0109 m/s	T_c	6.7^oC
γ	0.6	RH	60 %

Table 1: Physical properties of the experiment.

	e 24h	m 24 h	e 72h	m 72 h	e 92h	m 92h
top	15.5	15.5	11.0	11.5	9.4	9.6
middle	11.8	13.0	6.8	7.7	6.7	7.2
bottom	6.7	6.7	6.7	6.7	6.7	6.7

Table 2: Comparison of predicted and measured air temperatures (^oC) in the bulk at different times. The experimental data are taken from [24]. Here m and e denote the model and experiment.

4 Separation of timescales

4.1 Behavior of the product temperature

Since the experimental setup in the previous section is a specific one without interaction between $T_a(L,t)$ and $T_0(t)$, we will use a more general parameter choice in the following (Table 3). The transfer function $G_p^R(s)$ connects the input $\widehat{T}_a(x,s)$ to $\widehat{T}_p(R,x,s)$ (the Laplace transformed product surface temperature), and is approximated with a first order Padé method (as explained in subsection 2.2. The left hand side plot in Figure 3 shows the Bode magnitude

plots of $G_p^R(s)$ (with $s = j\omega$) from equation (16) and its first order approximation $\widehat{G}_p^R(s)$. The static gains are (per definition, see Appendix A.1) equal, and the time constant of $\widehat{G}_p^R(s)$ is accurate. The corner frequency is approximately at $\omega = 10^{-3} - 10^{-4}$ Herz, which indicates a time constant of order $10^3 - 10^4$ seconds. The time constant of the product temperature is by definition 1/6 of the time that it needs to reach it equilibrium value after a step input, [14] pp 292-293. Therefore the product temperature settles in hours. $G_p^0(s)$ is the transfer function that connects the input $\widehat{T}_a(x,s)$ to $\widehat{T}_p(0,x,s)$ (the

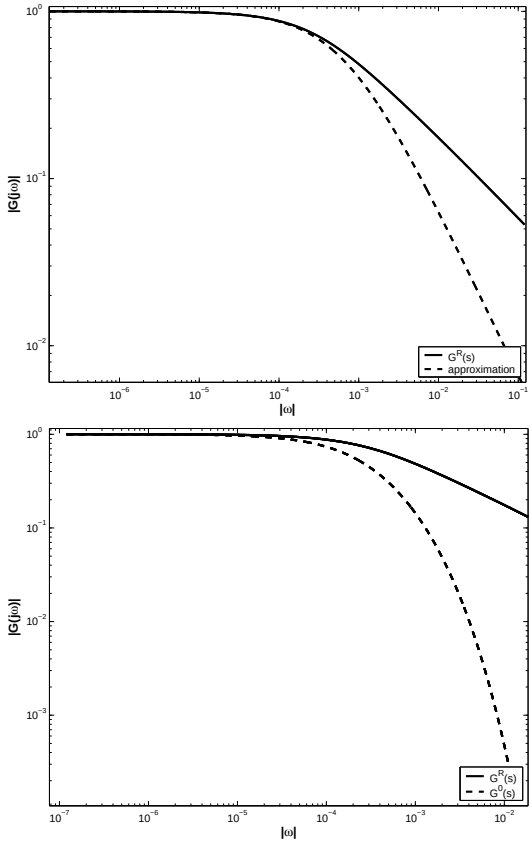

Figure 3: Left: the static gain and the time constant of the first order approximation of $G_p^R(s)$ are accurate. Right: the time constants of $G_p^R(s)$ and $G_p^0(s)$ are of the same order.

Laplace transformed core temperature). The right hand side plot in Figure 3 shows $G_p^0(s)$ and $G_p^R(s)$. The orders of their time constants are equal, and we conclude that the time constant of $T_p(0,x,t)$ is of the same order as that of $T_p(R,x,t)$. This is not surprising, since the skin temperature will not settle before the core temperature does. The strong descent of $G_p^0(s)$ for high s in-

dicates that the core temperature $T_p(0,x,t)$ barely responds to high frequency fluctuations in $T_a(x,t)$. Intuitively, this is not surprising, but analytically this is hard to see because of the complex form of $G_p^0(s)$. The difference in gain is less than 10 % for all frequencies, so the variation in T_p is always less than 10% of the variation in T_a. Further, the static gains of $G_p^0(s)$ and $G_p^R(s)$ are almost identical, and this can be seen analytically from the steady state of equations (12)–(14), that is

$$\frac{\frac{1}{2}\mathrm{NuM_3}}{-\sin(M_3)+M_3\cos(M_3)+\frac{1}{2}\mathrm{Nu}\sin(\mathrm{M_3})} \quad \text{and}$$
$$\frac{\frac{1}{2}\mathrm{Nu}\ \sin(\mathrm{M_3})}{-\sin(M_3)+M_3\cos(M_3)+\frac{1}{2}\mathrm{Nu}\sin(\mathrm{M_3})}, \tag{26}$$

respectively. Since M_3 is of the order of 10^{-2} we have that $\sin(M_3) \approx M_3$. The static gains are approximately equal, and therefore the spatial temperature differences inside a product due to respiration will be negligible in the equilibrium situation. Altogether, we conclude that $T_p(R,x,t)$ and $T_p(0,x,t)$ will practically never have large differences. For convenience, we will from now on only look at $T_p(R,x,t)$, and denote it with $T_p(x,t)$.

4.2 Time constants of the air temperatures

After focusing on the product temperature, in this section we will further analyze the behavior of the air temperatures in the different compartments of the storage room. The time constants of $T_0(t)$ are obtained from the transfer functions that correspond to equation (22)

$$\begin{aligned}\widehat{T}_0(s) &= G_3(s)\widehat{T}_a(L,s)+G_4(s)\widehat{T}_c(s) \\ &= \frac{1-\alpha}{1+\frac{V}{\Phi}s}\widehat{T}_a(L,s)+\frac{\alpha}{1+\frac{V}{\Phi}s}\widehat{T}_c(s).\end{aligned} \tag{27}$$

The time constants are both equal to $\frac{V}{\Phi}$. Therefore, the time constant of this subsystem equals $\frac{V}{\Phi}$, which will be in the order of $10^0 - 10^1$. The transfer function corresponding to equation (23) is

$$\widehat{T}_a(x,s) = \exp\left(-\frac{s+M_4}{v}x\right)\Big(\int_0^x \frac{M_4}{v}\exp\left(\frac{s+M_4}{v}z\right)\widehat{T}_p(z,s)dz + \widehat{T}_0(s)\Big). \tag{28}$$

From this expression it is hard to derive a time constant. Therefore, we temporarily assume that $T_p(x,t)$ is uniform in x. This is justified by the fact that the uniformity of $T_p(x,t)$ will not change the settle time of the air temperature significantly. The approximated transfer functions corresponding to equation (23) now become

$$\widehat{T}_a(x,s) = G_1(s,x)\widehat{T}_0(s)+G_2(s,x)\widehat{T}_p(x,s), \tag{29}$$

with

$$\begin{aligned} G_1(s,x) &= \exp\left(-\frac{s+M_4}{v}x\right) \\ G_2(s,x) &= \frac{M_4(1-\exp\left(-\frac{s+M_4}{v}x\right))}{s+M_4}. \end{aligned} \tag{30}$$

They are not rational since they contain a time delay x/v. Hence, we cannot see their time constants directly. The Padé[0,1] approximations in $s = 0$ are of first order and do not alter the time constant. They are given by

$$\begin{aligned} G_1(s,x) &\approx \frac{1}{\exp\left(\frac{M_4x}{v}\right) + \frac{x}{v}\exp\left(\frac{M_4x}{v}\right)s} \\ G_2(s,x) &\approx \frac{2(\cosh(\frac{M_4x}{v})-1)}{\exp\left(\frac{M_4x}{v}\right) - 1 + \frac{1}{M_4}(\exp\left(\frac{M_4x}{v}\right) - 1 - \frac{M_4x}{v})s}, \end{aligned} \tag{31}$$

with M_4 the reaction constant of the product heat production $(1/s)$. The corresponding time constants are

$$\frac{x}{v} \quad \text{and} \quad \frac{\frac{1}{M_4}(\exp\left(\frac{M_4x}{v}\right) - 1 - \frac{M_4x}{v})}{\exp\left(\frac{M_4x}{v}\right) - 1}, \tag{32}$$

which are typically of order $10^0 - 10^1$. Note that the dimensionless number

$$M_5 = \frac{M_4L}{v}; \quad \frac{\text{chemical reaction rate}}{\text{convective heat transfer rate}} \tag{33}$$

is analogous to the Damköhler I number

$$\text{Da I} = \frac{\text{chemical reaction rate}}{\text{convective mass transfer rate}}. \tag{34}$$

The settle times for air temperatures are due to a transport delay. The static gain of $G_1(s,x)$ decreases exponentially with x and M_4, and that it increases exponentially with v. Changes in xM_4/v barely influence the static gain of $G_2(s,x)$. This implies that for higher xM_4/v, $T_a(x,t)$ is coupled stronger to $T_p(x,t)$ and less strong to T_c. So $T_a(0,t)$ will respond much stronger to variations in $T_c(t)$ than $T_a(L,t)$. In Subsection 4.4 this is further confirmed by a model simulation.

The time constants of $T_a(x,t)$ and $T_0(t)$ are typically three orders lower than that of $T_p(x,t)$. We expect that after a switch in T_c, $T_a(x,t)$ and $T_0(t)$ will settle quickly, whereafter it will move slowly together with $T_p(x,t)$. When v is switched (and not T_c), the system is piecewise linear between two switches. This means that there is not one single transfer function that connects the input v to the output $T_p(x,t)$, so the analysis above does not apply. Nevertheless we expect that the difference between the time constants of the air and product temperatures will remain large. The assumption of a spatially uniform $T_p(x,t)$

in (28)–(30) seems strong. However, it is not a physically crucial assumption; it only simplifies the analysis mathematically.
This analysis is carried out per subsystem, i.e., for T_a, T_0, and T_p individually. In reality, these subsystems are coupled. This complicates the analysis considerably. However, we expect no dramatic effects due to the coupling and the non-uniformity in $T_p(x,t)$, but for confidence in the next sections numerical analysis that supports these expectations, is carried out on the nominal system with realistic parameters.

4.3 State space analysis

Let us consider the dynamics of the nominal system, described by equations (22)–(25), by means of eigenvalue analysis and time simulation. The equations are made discrete as follows. The term $v\frac{\partial T_a(x,t)}{\partial x}$ in equation (23) is upwind approximated like $v\frac{T_{a,n}-T_{a,n-1}}{\delta x}$, where the second subscript denotes the discrete space, starting from the bulk bottom. The spatially discretised full system is of the form

$$\frac{\partial T}{\partial t} = A_{full}(v)T + B_{full}(v)T_c, \tag{35}$$

with $T = [T_{a,1}..T_{a,n}\ T_0\ T_{p,1}..T_{p,n}]^T$. This differential equation is simulated in Simulink with the ode45 Dormand-Prince algorithm. The physical parameters of the chosen configuration are listed in Table 3. The heat capacity of the air is adjusted for humidity, by relating heat capacity to enthalpy change for air between 7 ^oC and 10 ^oC with a 90-95% relative humidity. The obtained value, 2 10^3, is also suggested in [15], chapter 13. For our parameter choice, Re = 2.17 10^2, so that we may use equation (6). For clarity, the system is discretised in only two spatial components: $n = 2$. For a system of the form

α	0.4	A_f	5 m
R	3.25 10^{-2} m	V	10 m^3
L	4 m	v	0.2 m/s
λ_p	0.55 $J/s\ m\ K$	ρ_p	1014 kg/m^3
a	3.1 10^{-5} $J/s\ kg\ K$	A_p	40 m^2
γ	0.31	c_p	3.6 10^3 $J/kg\ K$
T_c	275 K	c_a	2 10^3 $J/kg\ K$

Table 3: Physical parameters of a bulk with potatoes. The data specific for potato were taken from [10, 24].

(35), the negative inverses of the (real parts of the) eigenvalues of A_{full} represent the time constants of the system. The (real parts of the) eigenvalues of A_{full} are shown in the top row of Table 4. These eigenvalues contain small imaginary parts. This is probably due to the high condition number of $A_{full}(v)$ of $\mathcal{O}(10^7)$. Time simulation therefore shows small oscillations for any number of n, but when the state vectors $[T_{p,1},\ldots,T_{p,n}]^T$, $[T_0]$, and $[T_{a,1},\ldots,T_{a,n}]^T$ are simulated in parallel, the oscillations do not show up. The (real parts of the) eigenvectors

eigenvalue	-1.7e-5	-6.7e-5	-0.4	-0.4	-0.02
$T_{a,1}$	0.4	-0.2	- 0.01	-0.01	0.4
$T_{a,2}$	0.5	0.3	1.0	1.0	0.2
T_0	0.3	0.2	-0.04	-0.04	0.9
$T_{p,1}$	0.4	-0.6	0.8e-5	0.8e-5	-0.2e-2
$T_{p,2}$	0.6	0.7	-0.3e-3	-0.3e-3	-0.9e-3

Table 4: The eigenvalues are listed in the top row. The columns below the eigenvalues are the eigenvectors. The state space is $[T_{a,1}\ T_{a,2}\ T_0\ T_{p,1}\ T_{p,1}]$.

of the full system are shown as the columns below the eigenvalues in Table 4. The two left eigenvectors correspond to the small eigenvalues and thus to the slow dynamics, and the three right eigenvectors correspond to the large eigenvalues and thus to the fast dynamics. The only eigenvectors that have substantial components in the directions $T_{p,1}(t)$ and $T_{p,2}(t)$, are the slow ones, so T_p has only slow dynamics. This is in agreement with the analysis of the uncoupled subsystems from the previous section. The two slow eigenvectors also have substantial components in all the other directions, so the states T_0, $T_{a,1}$, and $T_{a,2}$ also have slow dynamics. The three fast eigenvectors have large components in the directions T_0, $T_{a,1}$, and $T_{a,2}$, so these states have also fast dynamics. We conclude that the dynamics of T_a, T_0 and T_p are coupled to each other: After a change of input, T_a and T_0 will settle quickly and then slowly move together with T_p. From the inverse eigenvalues we see that the time constants of the slow states are $\mathcal{O}(10^3)$, and that the time constants of the fast states are $\mathcal{O}(10^0)$. The rate of heat transfer, and therefore the rate of change of the system states depends strongly on v. However, for different choices of v, namely 0.1 and 10, similar results were obtained. The minus sign in the fourth row of the second eigenvector in Table 4 indicates that the temperature profile of $T_p(x,t)$ is spatially not uniform since the $T_{p,1}$ and $T_{p,2}$ move in opposite directions according to the second eigenvector. The time simulation in the next section shows that the air and product temperatures move together in one direction mainly, which implies that the first eigenvector is dominant.

4.4 Time simulation

The difference in timescales is visualized by a time simulation of $T_a(L,t)$, $T_a(0,t)$, $T_p(L,t)$, and $T_p(0,t)$. $T_c(t)$ is switched once every fifteen minutes between 275 K and 285 K. In all the simulations $n = 20$ layers was used, which was found to be quite accurate. The rest of the parameters are listed in Table 3. Figure 4 shows the fast and slow dynamics of $T_a(L,t)$ and $T_a(0,t)$, and the slow dynamics of $T_p(L,t)$ and $T_p(0,t)$: after a switch $T_a(L,t)$ and $T_a(0,t)$ settle quickly, whereafter they slowly move with $T_p(L,t)$ and $T_p(0,t)$. Since $T_p(L,t)$ and $T_p(0,t)$ are both at their equilibrium values, they hardly move and only the fast dynamics of $T_a(L,t)$ is visible. $T_p(L,t)$ is a bit higher than $T_p(0,t)$ due to the warming up of $T_a(x,t)$ inside the bulk. We observe that the fast dynamics of T_a and T_0

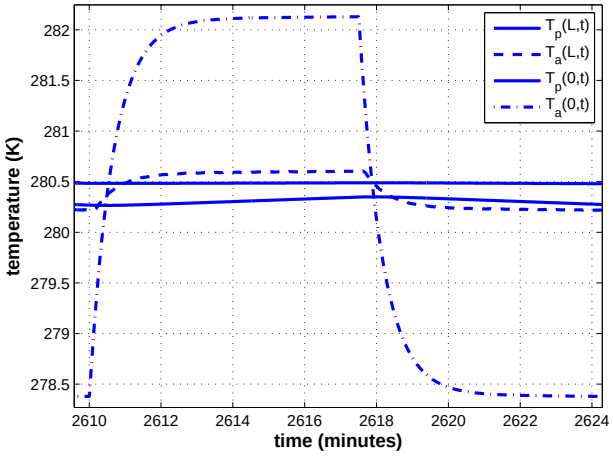

Figure 4: From top to bottom: the dynamics of $T_p(L,t)$, $T_a(L,t)$, $T_p(0,t)$, and $T_a(0,t)$. The input $T_c(t)$ is switched every fifteen minutes.

(not shown) are negligible on a timescale of fifteen minutes. This allows us to further simplify the model in the next section. We also observe that $T_a(0,t)$ responds much stronger on changes in $T_c(t)$ than $T_a(L,t)$, as was predicted in Subsection 4.2. As a consequence, $T_p(0,t)$ moves more than $T_p(L,t)$ during a switching interval.

5 Settle time for the bulk temperature

Given the results from the previous sections we will now focus on the behavior of the product temperature in the bulk under cooling and ventilation. Notice therefore that if a system is dominated by first order dynamics, the settle time can be predicted accurately by the time constant of a first order approximated system. We look at the time constant of the product surface rather than the product core, since in Subsection 4.1 we have shown that these two time constants are of the same order. We exploit the differences in timescales. The cooling down of the bulk is a slow process. Due to their fast dynamics, T_a and T_0 settle quickly to their equilibrium values, and slowly move along with T_p. Under quasi-steady state conditions the time derivative in (22) and (23) are set to zero. This is equivalent to neglecting the fast dynamics of T_a and T_0, which are only apparent at high frequencies or at short timescales. This leads to the

approximation

$$\begin{aligned} 0 &= -\alpha(T_a(L,t) - T_c(t)) + T_a(L,t) - T_0(t) && (36)\\ 0 &= -\frac{\partial T_a(x,t)}{\partial x} + \frac{M_4}{v}(T_p(x,t) - T_a(x,t)) && (37)\\ T_a(0,t) &= T_0(t)\\ \frac{\partial T_p(x,t)}{\partial t} &= A_p T_p(x,t) + B_p T_a(x,t). && (38) \end{aligned}$$

Laplace transformation of (38), and substituting this in (37) gives

$$\begin{aligned} \frac{\partial \widehat{T}_a(x,s)}{\partial x} &= \frac{M_4}{v}\left(\frac{B_p \widehat{T}_a(x,s)}{-A_p + s} - \widehat{T}_a(x,s)\right) && (39)\\ \widehat{T}_a(0,s) &= \widehat{T}_0(s) && (40)\\ \Rightarrow \widehat{T}_a(L,s) &= \widehat{T}_0 \exp\left(\frac{M_4 L}{v}\left(\frac{B_p}{-A_p+s} - 1\right)\right) && (41)\\ &= \left(-\alpha(\widehat{T}_a(L,s) - \widehat{T}_c(s)) + \widehat{T}_a(L,s)\right) * \\ &\quad \exp\left(M_5 \frac{B_p}{-A_p+s} - 1)\right), && (42) \end{aligned}$$

where we have used (36) and (33). Consequently,

$$\widehat{T}_a(L,s) = \frac{\alpha \exp\left(M_5\left(\frac{B_p+A_p-s}{-A_p+s}\right)\right)}{1-(1-\alpha)\exp\left(M_5\left(\frac{B_p+A_p-s}{-A_p+s}\right)\right)}\widehat{T}_c(s). \quad (43)$$

A Pade[0,1] approximation results in a first order system

$$\begin{aligned} \widehat{T}_a(L,s) &= \frac{\frac{\alpha A_p^2}{M_5 B_p}\exp\left(M_5\left(\frac{B_p+A_p}{-A_p}\right)\right)}{\frac{A_p^2}{M_5 B_p} - \frac{A_p^2(1-\alpha)}{M_5 B_p}\exp\left(M_5\left(\frac{B_p+A_p}{-A_p}\right)\right) + s}\widehat{T}_c(s)\\ &= \frac{\tilde{B}_p}{-\tilde{A}_p + s}\widehat{T}_c(s). && (44) \end{aligned}$$

Laplace transformation of equation (38) gives

$$\widehat{T}_p(L,s) = \frac{B_p}{-A_p+s}\widehat{T}_a(L,s). \quad (45)$$

So the transfer function from $\widehat{T}_c(s)$ to $\widehat{T}_p(L,s)$ equals

$$\frac{\tilde{B}_p B_p}{\tilde{A}_p A_p - (\tilde{A}_p + A_p)s + s^2}. \quad (46)$$

The Padé[0,1] approximation of this transfer function has a time constant of

$$-\frac{\tilde{A}_p + A_p}{\tilde{A}_p A_p}. \tag{47}$$

The settle time is defined as six times the inverse of the time constant, and is the time after which the temperature is more or less at its steady state. Figure 5 shows the time simulation of the cooling down of $T_p(L,t)$ and $T_p(0,t)$,

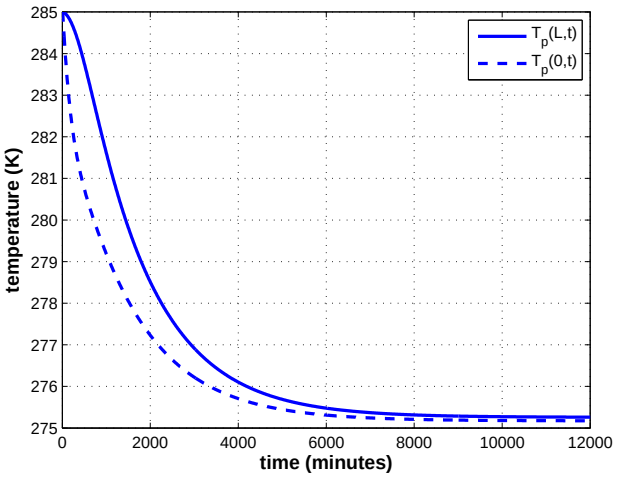

Figure 5: The settle time for $T_p(L,t)$ and $T_p(0,t)$ is about 10000 minutes. The uniform initial value is $T_p(x,0) = 285\ K$.

according to the system equations (22)–(25), with $T_c = 275$, $v = 0.2$, and the rest of the parameters are listed in Table 3. The settle time of $T_p(L,t)$ that is predicted by (47)is 10861 minutes, which is in agreement with the simulation results. The settle times for $T_p(L,t)$ and $T_p(0,t)$ are practically equal. The first order dynamics are dominant on a large time scale, which ensures an accurate prediction of the time constant and thus of the settle time of the system, but right after the start the effects of the higher order dynamics comes into play. The decay of $T_p(L,t)$ is somewhat slower in the beginning than that of $T_p(0,t)$, and is caused by the uniform initial bulk temperature. Consequently, the air at the top is heated up by the rest of the bulk, and the top products are cooled down very little. After a while, the bottom and middle of the bulk are cooled down and the air at the top gets less heated up than in the beginning. The air now starts cooling down the products at the top. Similar observations were made in [24].
The transfer function in equation (44) represents an unstable system if the signs

in the denominator are unequal, i.e., if

$$A_p^2 - A_p^2(1-\alpha)\exp\left(M_5\left(\frac{B_p + A_p}{-A_p}\right)\right) \leq 0. \tag{48}$$

Note that $A_p < 0$. Technically, this will give a chain reaction in which T_p starts rising, which induces more heat production, which causes T_p to rise further. In reality, heat production is finite, and the temperature will stop rising after some or all products have rotted away. This situation will practically only occur if α is very close to zero, indicating very poor cooling.

6 Calculation of the switching time

Because T_p has its highest values at the top of the bulk, we want to control $T_p(L,t)$. Our starting point is that $T_p(L,t)$ is at its optimal equilibrium value $T_{p,opt}$. In Subsections 4.1 and 4.2 we assumed piecewise constant inputs, which makes the analysis easier. The control problem consists of finding the optimal time to switch between these inputs. The inputs are switched between two discrete values, $(T_{c,1}, v_1)$ and $(T_{c,2}, v_2)$ once in an intermediate time interval of about ten minutes. The choice of this time interval has two reasons. Firstly, the air temperatures settle within a minute, so we can approximate them by constant values on this time interval (equations (36) and (37)). Secondly, T_p will move very slowly, so on a ten minute time scale its dynamics will be linear (first order) in time. The question is when to switch T_c or v (or both) such that $T_p(L,t)$ returns at its optimal value after each time interval. To determine the first order dynamics of $T_p(L,t)$, the transfer functions in equations (43) and (45) are combined and Padé[0,1] approximated to

$$\begin{aligned} \widehat{T}_p(L,s) &= \frac{\tilde{B}_p B_p}{\tilde{A}_p A_p - (\tilde{A}_p + A_p)s}\widehat{T}_c(s) && (49)\\ &= \frac{B_p^*}{-A_p^* + s}\widehat{T}_c(s), && (50) \end{aligned}$$

with

$$\begin{aligned} A_p^* &= \frac{\tilde{A}_p A_p}{A_p + \tilde{A}_p}\\ B_p^* &= -\frac{\tilde{B}_p B_p}{A_p + \tilde{A}_p}. \end{aligned}$$

The (approximated) first order dynamics of T_p are thus given by

$$\frac{dT_p(L,t)}{dt} = A_p^* T_p(L,t) + B_p^* T_c(t). \tag{51}$$

The solution to equation (51) at time τ is

$$\begin{aligned} T_p(L,\tau) &= T_p(L,0)\exp(A^*_{p,1}\tau) \\ &\quad + \int_0^\tau \exp(A^*_{p,1}(t-\tau))B^*_{p,1}T_{c,1}dt \qquad (52) \\ &= T_p(L,0)\exp(A^*_{p,1}\tau) \\ &\quad + \frac{B^*_{p,1}}{A^*_{p,1}}T_{c,1}(1-\exp(-A^*_{p,1}\tau)). \qquad (53) \end{aligned}$$

The second subscript refers to the discrete input v_1. Because $A^*_{p,1}\tau \ll 1$, we can accurately linearize this to

$$\begin{aligned} T_p(L,\tau) &\approx T_p(L,0)(1+A^*_{p,1}\tau) \\ &\quad + B^*_{p,1}T_{c,1}\tau \qquad (54) \\ \Rightarrow \frac{T_p(L,\tau)-T_p(L,0)}{\tau} &\approx A^*_{p,1}T_p(L,0) + B^*_{p,1}T_{c,1}, \qquad (55) \end{aligned}$$

which is equivalent to a forward Euler discretization in time. Similarly, but now with a backward Euler discretization, we get

$$\frac{T_p(L,\tau_f)-T_p(L,\tau)}{\tau_f-\tau} \approx A^*_{p,2}T_p(L,\tau_f) + B^*_{p,2}T_{c,2}. \qquad (56)$$

Together with the condition $T_p(L,0) = T_p(L,\tau_f) = T_{p,opt}$, where $T_{p,opt}$ is the optimal equilibrium value, this leads to

$$\begin{aligned} 0 =& \tau(A^*_{p,1}T_{p,opt} + B^*_{p,1}T_{c,1}) \\ &+ (\tau_f-\tau)(A^*_{p,2}T_{p,opt} + B^*_{p,2}T_{c,2}). \qquad (57) \end{aligned}$$

Simple calculus gives the optimal switching time τ_{opt}

$$\tau_{opt} = -\tau_f \frac{A^*_{p,2}T_{p,opt} + B^*_{p,2}T_{c,2}}{(A^*_{p,1}-A^*_{p,2})T_{p,opt} + B^*_{p,1}T_{c,1} - B^*_{p,2}T_{c,2}}. \qquad (58)$$

To see whether this switching time will lead $T_p(L,t)$ to its optimal value, we look at the transfer functions once more. Figure 6 shows the transfer functions from $\widehat{T}_c(s)$ to $\widehat{T}_p(L,s)$ of system (22)–(25), and of the approximated system (49). The first order dynamics of both systems are equal. The gain difference is typically less than 10 % for all frequencies. If we consider v to be constant throughout, than fluctuations of T_c will result in a maximal error in amplitude of $T_p(L,t)$ of 10 %. The maximal phase error can be a quite large for low air velocities, which means that the predicted output signals of a sinusoidal input can differ more than one period. Since the static gains of both systems are equal (which is inherent to a Padé approximation), the average value of the $T_p(L,t)$ will for both systems be the same. Since a switched input signal is the infinite sum over sinusoidal inputs, we expect that the optimal switching time from (58) will lead

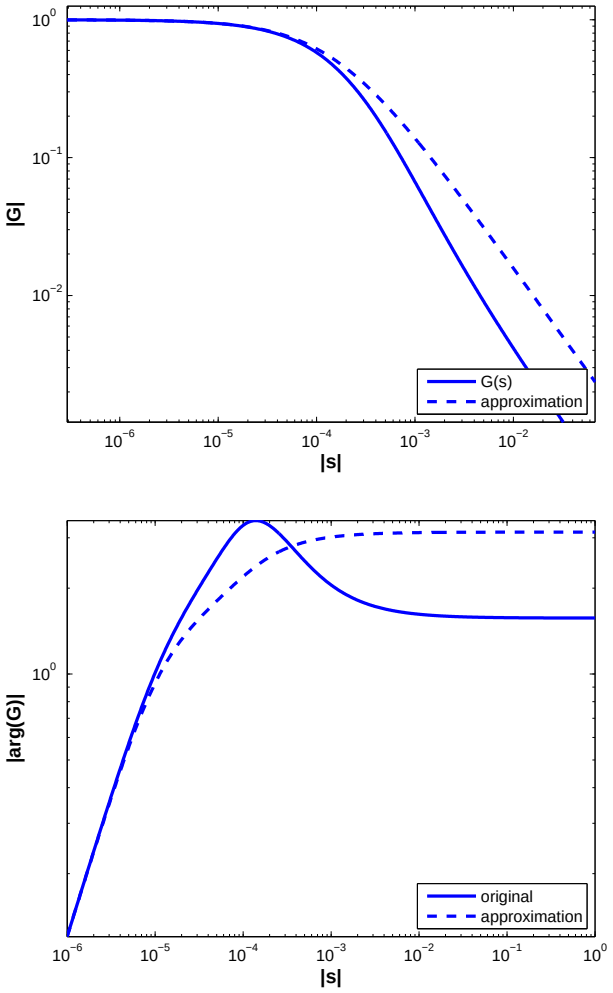

Figure 6: The difference in gain (left) between the nominal and the approximated system are small. The phase differences can become quite large for low air velocities (right).

$T_p(L,t)$ in the nominal model to $T_{p,opt}$. This is confirmed by simulations. When not only T_c varies, but also v, the analysis given above will not hold anymore, since the temperature dynamics are described by two systems. However, since for both systems the transfer functions of the nominal and the approximated model have the same first order dynamics, we expect that $T_p(L,t)$ will attain $T_{p,opt}$ using the proposed switching moment. Simulations show that when both v and T_c are switched, (58) leads $T_p(L,t)$ very nearly to $T_{p,opt}$. As an example, Figure 7 shows the simulated dynamics of $T_p(L,t)$ of the nominal model. The

switching time is derived from the approximated model. Each time interval $[0, \tau_f]$ with $\tau_f = 10$ minutes, the inputs are switched once, such that in each interval input 1 is applied for τ seconds, and input 2 is applied for $\tau_f - \tau$ seconds. We have $T_{c,1} = 275\ K$, $T_{c,2} = 285\ K$, $v_1 = 0.2\ m/s$, and $v_2 = 0.02\ m/s$. The rest of the physical coefficients are listed in Table 3. For $\tau = \tau_{opt}$, $T_p(L,t)$ moves slowly around its equilibrium value of 279.79 K. Since $T_{p,opt} = 280\ K$, there is an error of 0.21 degrees.

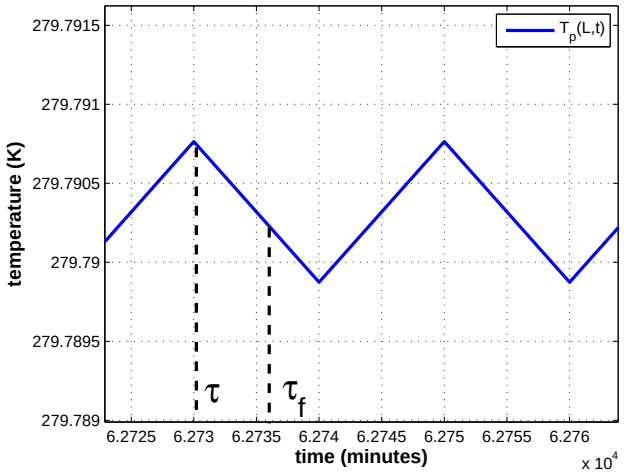

Figure 7: $T_p(L,t)$ moves slowly around its equilibrium value of 279.79 K. The difference with the optimal product temperature is 0.21 K.

6.1 Cooling block as control mechanism

Figure 8 shows that if $T_p(L,t)$ is far away from $T_{p,opt}$, it will move towards it using τ_{opt}. This results in the same small error between $T_p(L,t)$ and $T_{p,opt}$ as in the previous section. Mathematically, it is hard to analyze the stability of a switching system. However, there is an intuitive explanation to this phenomenon: the cooling element acts as a stabilizing control mechanism, since equation (3) implies that a higher $T_a(L,t)$ is cooled down more, and a lower $T_a(L,t)$ is cooled down less. The difference between $T_p(L,t)$ and $T_{p,opt}$ becomes larger for smaller values of v_2; this is because the settle time of T_a increases and starts violating the assumption that the fast dynamics of T_a can be neglected. During v_2, T_a heats up very slowly, so on average T_a will be lower than predicted.

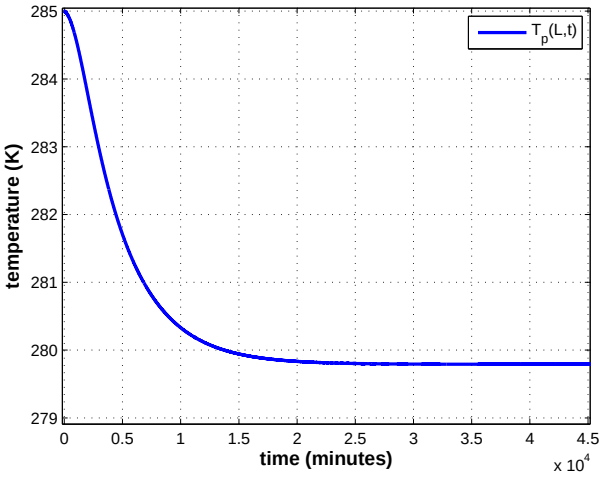

Figure 8: From an arbitrary initial value of 285 K, the product temperature at the top of the bulk converges close to its optimal value of 280 K. The difference is 0.2 K.

6.2 Lumped system approach

In this section the advantage of a delicately modelled heat transfer mechanism is explained. In [15] chapter 13, and [21] chapter 6.6.1, models for a bulk storage room without spatial variabilities were used. The ventilation strategy was designed on (amongst others) the total heat production of the bulk. Using these assumptions in our model, the temperature dynamics are described by

$$V_a \rho_a c_a \frac{dT_a(t)}{dt} = \rho_p V_b T_p(t) a - \rho_a \Phi \alpha (T_a(t) - T_c), \tag{59}$$

with V_a the total air volume in the shaft and bulk, and V_b the total product volume. A solution strategy similar to the one used in equations (54)–(58) results in

$$\tau_{opt} = \tau_f \frac{c_1 - c_{22}(T_{a,opt} - T_c)}{c_{21}(T_{a,opt} - T_c) + c_{22}(T_{a,opt} - T_c)}, \tag{60}$$

with $c_1 = \frac{a \rho_p V_b T_{p,opt}}{V_a \rho_a c_a}$, $c_{21} = \frac{\rho_a \Phi_1 \alpha}{V_a \rho_a}$, and $c_{22} = \frac{\rho_a \Phi_2 \alpha}{V_a \rho_a}$. The resulting τ is only a fraction of the value of τ in equation (58), and resulted in too little cooling. The cause of this is that the transport of respiration heat from the bulk to the heat exchanger is hindered by the heat transfer resistance between products and air, and the transport time of bulk air to the heat exchanger. The heat transport is accelerated by more air circulation. Repeating the simulation experiment in subsection 6.1 with switching time (**??**), results in product temperatures that are 5 degrees too high.

7 Conclusions

We have modelled a storage room in a basic way, maintaining the most essential physical properties. The resulting system equations are first validated experimentally, and then mathematically simplified using timescale decomposition, discrete switching input, and Padé approximations of transfer functions. The transfer functions of the simplified system give a good indication of the timescales, and also show how the fast states are coupled to the slow ones. These properties are supported by analysis and simulation of the nominal system. This simplifies the system in such a way, that a control law for the switching input, and the settle time for the bulk temperature are in complete parametric form. The mathematical techniques reduce the complexity of the model, but the first order dynamics that are most important, are maintained. This results in an accurate prediction of the optimal switching time of the input and the settle time of the bulk temperature, which is confirmed by simulations of the nominal model. The parametric expressions give a lot of information about the sensitivities to different parameters. The optimal switching time gives an impression on the optimal choice of v_1, v_2, $T_{c,1}$, and $T_{c,2}$. These design parameters should be chosen such that $\tau_{opt}/\tau_f \approx 1/2$, so the switching time can be adjusted for model errors and disturbances.

8 Acknowledgement

This work was supported by the Technology Foundation STW under project number WWI.6345.

Appendix

A.1 Construction of an irrational transfer function and its Padé approximation

A transfer function of a linear pde in the variables x and t is constructed by substituting $\partial/\partial t = s$ and solving the ode for the variable x. The solution can be written as $\widehat{y}(s,x) = G(s,x)\widehat{u}(s,x)$, with $\widehat{y}(s,x)$, $\widehat{u}(s,x)$ and $G(s,x)$ the output, input and the transfer function, respectively.
If $G(s,x)$ is of the form

$$\frac{a_0 s^0 + .. + a_n s^n}{b_0 s^0 + .. + b_m s^m}, \tag{61}$$

i.e. rational, then the transfer function for a fixed x can be transformed back into a linear ode in t, and its time constant can be determined. If not, the nonrational transfer function can be approximated by a rational one, for example by a Padé approximation. A Padé[0,1] approximation of $G(s,x)$ in $s = 0$ is of the form

$$\tilde{G}(s,x) = \frac{1}{a_1(x) + a_2(x)s}, \tag{62}$$

where the coefficients $a_1(x)$ and $a_2(x)$ are determined by setting

$$\begin{aligned} G(0,x) &= \tilde{G}(0,x) \\ \frac{\partial G}{\partial s}(0,x) &= \frac{\partial \tilde{G}}{\partial s}(0,x). \end{aligned}$$

A clever choice of the orders n and m in a Padé$[n,m]$ approximation is made by observation of the Bode plot of the original transfer function.

A.2 Notation

Φ	air flow through shaft (m^3/s)
α	cooling effectiveness (K)
α_{th}	thermal diffusivity of air $(1.87\ 10^{-5}\ m^2/s)$
γ	porosity (m^3/m^3)
λ_a	conduction of air $(2.43\ 10^{-2}\ W/m\ K)$
λ_p	conduction of product $(W/m\ K)$
ν	kinematic viscosity of air $(1.3465\ 10^{-5}\ m^2/s)$
ρ_a	air density $(1.27\ kg/m^3)$
ρ_p	produce density (kg/m^3)
τ	switching time (s)
τ_f	length of switching interval (s)
A_f	floor area of the bulk (m^2)
A_p	produce surface per bulk volume (m^2/m^3)
Bi	Biot number $\frac{2hR}{\lambda_a}$
L	bulk height (m)
L_2	$R * \gamma(1-\gamma)$, char. length (m)
M_1	$\frac{\lambda_p}{\rho_p c_p}$
M_2	$\frac{a}{c_p}$
M_3	$\sqrt{M_2/M_1}R$
M_4	$\frac{hA_p}{\gamma\rho_a c_a}$
M_5	$\frac{M_4 L}{v}$
Nu	Nusselt number $\frac{2hR}{\lambda_a}$
Pr	Prandtl number $\frac{\nu}{\alpha_{th}}$
R	product radius (m)
Re	Reynolds number $\frac{vL_2}{\nu}$, see [24]
T_a	air temperature in the bulk (K)
T_c	cooling element temperature (K)
T_{ini}	initial temperature (K)
T_p	produce temperature
V	volume of shaft (m^3)
a	product heat production $(J/kg\ s\ K)$
b	product heat production $(J/kg\ s)$
c_a	heat capacity of air $(1\ 10^3\ J/kg\ K)$
c_p	heat capacity of produce $(J/kg\ K)$
h	heat transfer coefficient (W/m^2K)
v	air velocity inside the bulk (m/s)

References

[1] A.A. Alonso, J.R. Banga, and I. Sanchez. Passive control design for distributed process systems: theory and applications. *AIChE Journal*, 46(8):1593–1606, 2000.

[2] M.K. Chourasia and T.K. Goswami. Simulation of transport phenomena during natural convection cooling of bagged potatoes in cold storage, part i: fluid flow and heat transfer. *Biosystems engineering*, 94(1):33–45, 2006.

[3] M.K. Chourasia and T.K. Goswami. Simulation of transport phenomena during natural convection cooling of bagged potatoes in cold storage, part ii: mass transfer. *Biosystems engineering*, 94(2):207–219, 2006.

[4] P.D. Christofides. Control of nonlinear ditributed process systems: recent developments and challenges. *AIChE Journal*, 47(3):514–518, 2001.

[5] P.D. Christofides. *Nonlinear and robust control of of PDE systems: methods and applications to transport-reaction processes*. Birkhäuser: Boston, 2001.

[6] S. Dubljevic, P.D. Christofides, and I.G. Kevrekidis. Distributed nonlinear control of diffusion-reaction processes. *International journal of robust and nonlinear control*, 14:133–156, 2004.

[7] K. Gottschalk. Mathematical modelling of the thermal behaviour of stored potatoes and developing of fuzzy control algorithms to optimise the climate in storehouses. *Acta horticulturae: technical communications of ISHS*, 10:331–340, 1996.

[8] K. Gottschalk and W. Schwarz. Klimaautomatisierung für kartoffellager. *Landtechnik*, 3:132–133, 1997.

[9] L. K. Gottschalk, I. Nagy, and Farkas. Improved climate control for potato stores by fuzzy controllers. *Computers and electronics in agriculture*, 40:127–140, 2003.

[10] K.J. Keesman, D. Peters, and L.J.S. Lukasse. Optimal climate control of a storage facility using local weather forecasts. *Control Engineering Practice*, 11:505–516, 2003.

[11] L.J.S. Lukasse, J.E. de Kramer-Cuppen, and A.J. van der Voort. A physical model to predict climate dynamics in ventilated bulk-storage of agricultural produce. *International Journal of Refrigeration*, 30:195–204, 2007.

[12] G.C. Misener and G.C. Shove. Simulated cooling of potatoes. *American society of agricultural engineers*, 19(5):967–969, 1976.

[13] H.B. Nahor, M.L. Hoang, P. Verboven, M. Baelmans, and B.M. Nicolai. Cfd model of the airflow, heat and mass transfer in cool stores. *International Journal of Refrigeration*, 28:368–380, 2005.

[14] J.W. Polderman and J.C. Willems. *Introduction to mathematical systems theory*. Springer-Verlag, 1998.

[15] A. Rastovski and A. van Es et al. *Storage of potatoes, Post-harvest behaviour, store design, storage practice, handling*. Pudoc Wageningen, 1987.

[16] A.K. Thompson. *Controlled atmosphere storage of fruits and vegetables*. CAB International, 1998.

[17] R.G.M. van der Sman. Simple model for estimating heat and mass transfer in regular- shaped foods. *Journal of food engineering*, 60:383–390, 2003.

[18] S. van Mourik, J. Ploegaert, H.J. Zwart, and K.J. Keesman. Performance analysis of a temperature controlled bulk storage room. In *8th International Symposium on Dynamics and Control of Process Systems*. Dycops2007, June 2007.

[19] S. van Mourik, H.J. Zwart, and K.J. Keesman. Switching control for post-harvest food storage. In *Modelling and Design of Control Systems in Agriculture*. Agricontrol 2007, October 2007.

[20] P. Verboven, D. Flick, B.M. Nicolai, and G. Alvarez. Modelling transport phenomena in refrigerated food bulks, packages and stacks: basics and advances. *International Journal of Refrigeration*, 29:985–997, 2006.

[21] G.J.C. Verdijck. *Product quality control*. PhD thesis, University of Eindhoven, 2003.

[22] S. Whitaker. Forced convection heat transfer correlations for flow in pipes, past flat plates, single cylinders, single spheres, and for flow in packed beds and tube bundles. *Journal of american institution of chemical engineers*, 18(2):361–371, 1972.

[23] Y. Xu and D. Burfoot. Predicting condensation in bulks of foodstuffs. *Journal of food engineering*, 40:121–127, 1999.

[24] Y. Xu and D. Burfoot. Simulating the bulk storage of foodstuffs. *Journal of food engineering*, 39:23–29, 1999.